

Human Motion Prediction via Spatio-Temporal Inpainting

A. Hernandez Ruiz¹ J. Gall² F. Moreno-Noguer¹

¹Institut de Robòtica i Informàtica Industrial, CSIC-UPC, Barcelona, Spain

² Computer Vision Group, University of Bonn, Germany

Abstract

We propose a Generative Adversarial Network (GAN) to forecast 3D human motion given a sequence of observed 3D skeleton poses. While recent GANs have shown promising results, they can only forecast plausible human-like motion over relatively short periods of time, i.e. a few hundred milliseconds, and typically ignore the absolute position of the skeleton w.r.t. the camera. The GAN scheme we propose can reliably provide long term predictions of two seconds or more for both the non-rigid body pose and its absolute position, and can be trained in a self-supervised manner. Our approach builds upon three main contributions. First, we consider a data representation based on a spatio-temporal tensor of 3D skeleton coordinates which allows us to formulate the prediction problem as an inpainting one, for which GANs work particularly well. Secondly, we design a GAN architecture to learn the joint distribution of body poses and global motion, allowing us to hypothesize large chunks of the input 3D tensor with missing data. And finally, we argue that the L2 metric, which is considered so far by most approaches, fails to capture the actual distribution of long-term human motion. We therefore propose an alternative metric that is more correlated with human perception. Our experiments demonstrate that our approach achieves significant improvements over the state of the art for human motion forecasting and that it also handles situations in which past observations are corrupted by severe occlusions, noise and consecutive missing frames.

1. Introduction

Recent advances in motion capture (MoCap) technologies, combined with large scale datasets such as Human3.6M [20], have spurred the interest for new deep learning algorithms able to forecast 3D human motion from past skeleton data. State-of-the-art approaches formulate the problem as a sequence generation task, and solve it using Recurrent Neural Networks (RNNs) [13, 21], sequence-to-sequence models [28] or encoder-decoder predictors [9, 15]. While the results of these works are very promising, they

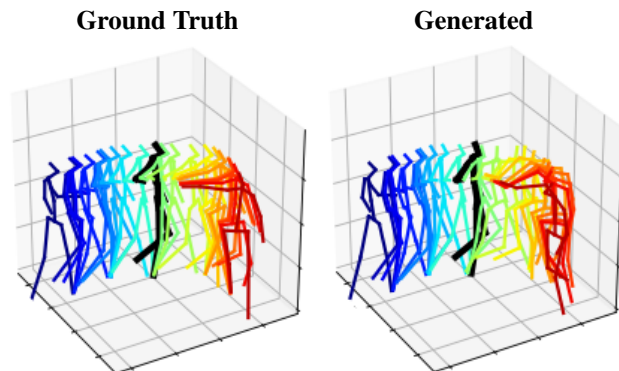


Figure 1. **Example result.** Our approach is the first in generating full body pose, including skeleton motion and absolute position in space. The predicted sequence starts from the skeleton marked in black. Note that the generated motion is somewhat different but semantically indistinguishable from the ground truth.

suffer from three fundamental limitations. First, all approaches address a simplified version of the problem in which global body positioning is disregarded, either by parameterizing 3D body joints in terms of position agnostic angles [13, 21, 28] or in terms of body centered Cartesian coordinates [9]. Second, most approaches require additional supervision in terms of action labels both during training and inference, which limits the applicability of these approaches to general motion sequences which do not correspond to the observed actions in the training data. And third, most approaches aim to minimize the L2 distance between the ground truth and generated motions. The L2 distance, however, is known to be an inaccurate metric, specially to compare long motion sequences. In particular, the use of this metric to train a deep network favors motion predictions that converge to a static mean pose. Even though this issue has been raised in [21, 15] and is partially solved during training using other metrics (e.g. geodesic loss), the L2 distance is still being used as a common practice when benchmarking different methodologies. To our understanding, this practice compromises the progress in this field.

In this paper we tackle all three issues. Specifically, we design a novel GAN architecture that is conditioned on

past observations and is able to jointly forecast non-rigid body pose and its absolute position in space. For this purpose we represent the observed skeleton poses (expressed in the camera reference frame) using a spatio-temporal tensor and formulate the prediction problem as an inpainting task, in which a part of the spatio-temporal volume needs to be regressed. A GAN architecture consisting of a fully convolutional generator specially designed to preserve the temporal coherence, and three independent discriminators that enforce anthropomorphism of the generated skeleton and its motion, makes it possible to render highly realistic long-term predictions (of 2 seconds or more). Interestingly, the L2 loss is only enforced over the reconstructed past observations and not over the hypothesized future predictions. This way, the generation of future frames is fully controlled by the discriminators. In fact, our model does not require ground truth annotations of the generated frames nor explicit information about the action being performed.

We also introduce a novel metric for estimating the similarity between the generated and the ground truth sequences. Instead of seeking to get a perfect match for all joints across all frames (as done when computing the L2 distance), the metric we propose aims to estimate the similarity between distributions over the human motion manifold. Concretely, a Linear Discriminant Analysis (LDA) model is learned from a random split of the training set. Ground truth and generated test samples are then projected onto the LDA manifold and their similarity estimated by means of the Spearman correlation coefficient. As it will be shown in the results section, this metric (dubbed LDA-SCC) captures more accurately the semantics of the human motion than the L2 distance. To empirically support the validity of LDA-SCC, we conducted a user study in which we showed the metric to be directly correlated with the human assessment about the realism of the rendered sequences.

In the experimental section we show that our approach, besides yielding full body pose, orientation and position, is also robust to challenging artifacts including missing frames and occluded joints on the past skeleton observations that condition our generative model. Fig. 1 shows an example result of our approach.

2. Related Work

Early approaches to modelling human motion. The inherent high-dimensionality and non-linearity of the human body motion makes the task of building statistical models very challenging. Traditional approaches have addressed the task using latent variable models such as Hidden Markov Models [6], bilinear spatio-temporal basis models [2], Gaussian processes [37, 38, 39], linear dynamic systems [30] and random forests [25]. These models, however, are based on relatively simple dynamics which are

only valid for short time predictions and are highly specialized on certain types of motion. Conditional Restricted Boltzmann Machines [33, 36, 35] capture better the nonlinearities of the human motion, although they are systems more complex to train and require sampling for inference.

Deep Learning for motion prediction. Most recent deep learning approaches build upon the problem formulation proposed by [36] in which input motion sequences are represented by a set of 3D body joint angles in a kinematic tree. Motivated by their success in machine translation problems [34, 10, 22], RNNs are then used to predict motion sequences of body joint angles. For instance, Fragkiadaki *et al.* [13] introduce an Encoder-Recurrent-Decoder (ERD) in combination with a Long Short-Term Memory (LSTM) for this purpose. Jain *et al.* [21] introduced structural RNNs, an approach that exploits the structural hierarchy of the human body parts. Martinez *et al.* [28] develop a sequence-to-sequence architecture with a residual connection that incorporate action class information via one-hot vectors. While well-suited for the particular motion they are trained for, these approaches do not generalize to other actions. More importantly, these models are only effective at predicting in the short- and mid-range time horizons, and are often surpassed by a simple zero velocity baseline model. This is in part due to the use of the L2 metric both for training and evaluation. More recent approaches have different strategies to address this problem.

Li *et al.* [26], propose a model with an auto-regressive CNN generator, and combine the L2 loss with an adversarial loss. Gui *et al.* [15] fully eliminate the L2 loss at training, and utilize an ERD model with a combination of an adversarial and geodesic losses. These works, however, still perform evaluation according to the L2 metric, which fail to capture the semantics of the motion, specially for long term predictions. Furthermore, since motion is parameterized in terms of the joint angles, the rotation and translation of the body in space is not estimated.

In this respect, Bütepage *et al.* [8] use fully-connected encoders to predict centered body coordinates, i.e. disregarding the absolute translation. Again, L2 loss is used at train. Instead of performing deterministic predictions, [9] and [4] model the probabilistic space of the joint coordinates, via Variable Auto Encoders (VAEs) and a Wasserstein GAN [16], respectively. Since these approaches do not produce a single output sequence, not direct comparison with the all above state-of-the-art is provided.

Sequence completion and image inpainting. Completing missing data within a sequence has been traditionally addressed using low-rank matrix factorization [40, 1]. Deep Learning approaches have also been used for this purpose *e.g.*, through RNNs [27, 24]. These works, however, are not designed for future prediction, which we have found as the most challenging case of completion.

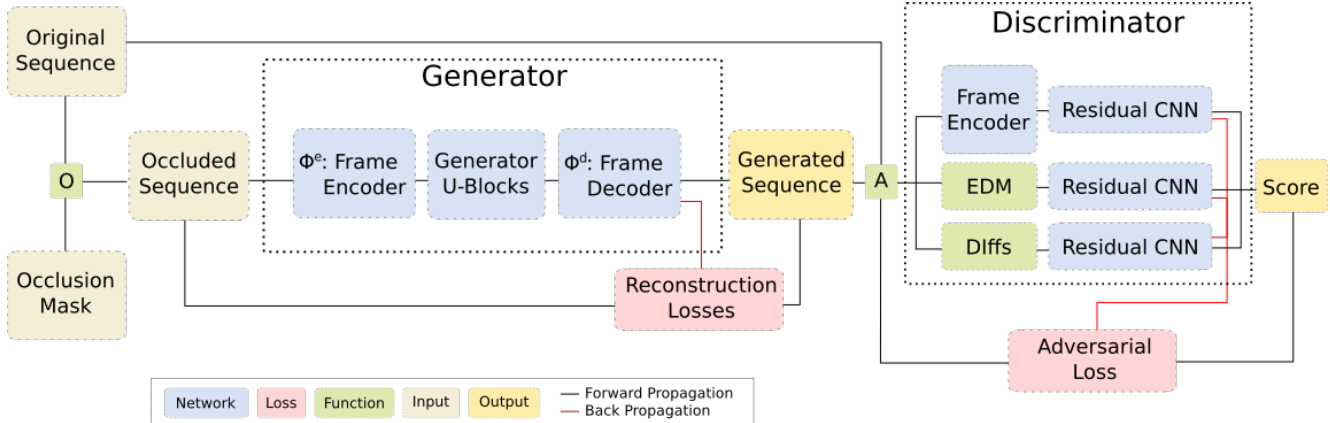


Figure 2. Overview of our Spatio-Temporal Motion Inpainting GAN (STMI-GAN) architecture. An input masked sequence of 3D joint coordinates is fed into a fully convolutional and time preserving generator. The output sequence is controlled by a number of geometric constraints, including losses applied to the generator output and adversarial losses of three independent discriminators.

Image inpainting is a very related problem. In the deep learning era, Denoising AEs [5] and Variational AEs [23] have become prevalent frameworks for denoising and completing missing data and image inpainting. These baselines, however, cannot handle large missing portions of structured data. State of the art has been significantly pushed by GANs conditioned with partial or corrupted images [31, 41, 42]. As we shall see, our approach draws inspiration on this idea.

Metrics for evaluating human motion prediction. The fact that simple metrics like L1 or L2 loss are not appropriate for measuring similarity between human motion sequences has been recently discussed in [15, 11]. A geodesic loss to train the network is proposed in [15] to address this issue, although the final evaluation is still done using L2. Coskun *et al.* [11] use deep metric learning and a contrastive loss to learn the metric directly from the data. In the same spirit, the metric we will introduce later also aims to compare the semantics of the sequences in a low dimensional motion manifold, which we compute in a supervised manner using Linear Discriminant Analysis.

3. Problem Formulation

We represent human pose with a J -joint skeleton, where each joint consists of its 3D Cartesian coordinates expressed in the camera coordinate reference frame. Rotation and translation transformations are inherently encoded in such coordinates. A motion sequence is a concatenation of F skeletons, which we shall represent by a tensor $\mathbf{S} \in \mathbb{R}^{F \times J \times 3}$. Let us also define an occlusion mask as a binary matrix $\mathbf{M} \in \mathbb{B}^{F \times J \times 3}$, which determines the part of the sequence that is not observed and is applied onto the sequence by performing the element-wise dot product $\mathbf{S} \circ \mathbf{M} \equiv \mathbf{S}^m$. Our goal is then to estimate the 3D coordinates of the masked joints. Note that depending on the pattern used to generate the occlusion mask \mathbf{M} , we can define

different sub-problems. For instance, by masking the last frames of the sequence we would have a forecasting problem; if instead we mask specific intermediate joints, then we would have random joints occlusions, structured occlusions or missing frames. The model we describe in the following section can indistinctly tackle any of these situations.

4. Model

4.1. STMI-GAN architecture

Fig. 2 shows an overview of the GAN we propose, in which we pose the human motion prediction problem as an inpainting task in the spatio-temporal domain. We denote our network as STMI-GAN (Spatio-Temporal Motion Inpainting GAN). We next describe its main components.

4.1.1 Generator

The rationale for the design holds in that convolutional GANs have been successful in image inpainting problems, which is similar to ours. A masked human motion sequence \mathbf{S}^m , however, cannot be directly processed by a convolutional network because the dimension corresponding to the joints (J) does not have a spatial meaning, in contrast to the temporal (F) and Cartesian coordinates dimensions. That is, neighboring joints along this dimension do not correspond to neighboring joints in 3D space¹.

To alleviate this lack of spatial continuity problem, the generator is placed in-between a frame autoencoder, namely a frame encoder Φ^e and a frame decoder Φ^d , which are symmetrical networks. The frame encoder, operates over the joint (J) dimension and projects each frame $\mathbf{S}_{i::}^m \in \mathbb{R}^{J \times 3}$ of the sequence to a one-dimensional vector $\mathbf{S}_{i::}^e = \Phi^e(\mathbf{S}_{i::}^m) \in$

¹For instance, the joint #0 is normally the hip, and its neighbors in the body graph are the joints #1 (left hip), #5 (right hip) and #9 (spine).

$\mathbb{R}^{H \times 1}$, where H is the dimension of the space for the pose embedding². To project each frame, the encoder does not use information from neighboring frames, being thus time invariant.

We denote the encoded sequence as $\mathbf{S}^e \in \mathbb{R}^{F \times H \times 1}$.

This encoded sequence is then passed through a series of generator blocks Φ^g , which produces a new sequence $\mathbf{S}^g \in \mathbb{R}^{F \times H \times 1}$ in the embedded space. The blocks of the generators are CNNs that process the sequence in both temporal and spatial dimensions. Further details are explained in Section 6. Finally the decoder network Φ^d maps back the transformed sequence \mathbf{S}^g to the output sequence in the original shape $\mathbf{S}^{out} \in \mathbb{R}^{F \times J \times 3}$.

4.1.2 Discriminator

To capture the complexity of the human motion distribution we split the discriminator into three branches, capturing different aspects of the generated sequence. Each discriminator is concatenated to a Residual CNN classifier that outputs the probability of the sequence of being real. We next describe the main blocks of our model. Specificities of the underlying architectures are detailed later in Sect. 6.

Base discriminator. The same architecture of the frame encoder Φ^e , with independent parameters, is used to process the generated sequence \mathbf{S}^{out} . The reason to reuse such architecture is that we want a discriminator to be applied directly on the non Euclidean representation used by the CNN blocks of the generator, in order to boost its performance.

EDM discriminator. We introduce a geometric critic that evaluates the anthropomorphism of the generated sequence \mathbf{S}^{out} via the analysis of its Euclidean Distance Matrix, computed as $\text{EDM}(\mathbf{S}^{out}) \equiv \mathbf{D} \in \mathbb{R}^{J \times J}$, where \mathbf{D}_{ij} is the Euclidean distance between joints i and j of \mathbf{S}^{out} . This is known to be a rotation and translation invariant representation [18], allowing to focus the attention of the discriminator into the shape of the skeleton.

Motion discriminator. To model joint correlations between the absolute motion of joints in space their relative (articulated) motion we consider a third discriminator that operates over the concatenation of the temporal differences of absolute coordinates $\|\mathbf{S}^{out}(t) - \mathbf{S}^{out}(t-1)\|_1$ and the temporal differences of EDM representations $\|\text{EDM}(\mathbf{S}^{out}(t)) - \text{EDM}(\mathbf{S}^{out}(t-1))\|_1$, where $\mathbf{S}^{out}(t)$ indicates generated the sequence at time t .

4.2. Losses

To train our network we use two main losses: 1) The reconstruction losses, that encourage the generator to preserve the information from the visible part of the sequence; 2) The GAN loss, which guides the generator to inpaint the

sequences by learning and reproducing the motion in the dataset. For all the following formulae, let \mathbf{S} be the input motion sequence, \mathbf{M} the occlusion mask, \mathbf{S}^{out} the generated sequence, F number of frames and J number of joints.

Reconstruction Loss. Our default reconstruction loss computes the L2 norm over the generated sequence w.r.t. the visible portion of the ground truth.

$$\mathcal{L}_{rec} = \|(\mathbf{S}^{out} \circ \mathbf{M}) - (\mathbf{S} \circ \mathbf{M})\|_2 \quad (1)$$

This loss is only applied over the visible part of the original and generated sequences. By doing this we prevent our network to converge to an average sequence.

Limb Distances Loss. [18] showed that most common actions can be recognized from just the relative distance between the extremities, *i.e.* hands, feet and head. We therefore add a loss that explicitly enforces the correct distance between these semantically important joints. Since this loss looks at the relative distance, instead of the absolute position, it provides different gradients to the reconstruction loss, and encourages the network to learn a more precise location for the limbs. Formally, if we denote by $\mathcal{E} = \{i, j\}$ the set of limb pairs, the loss \mathcal{L}_{limb} is computed as:

$$\sum_{f=1}^F \sum_{\{i,j\} \in \mathcal{E}} \left| \|\mathbf{S}_{fi}^m - \mathbf{S}_{fj}^m\|_2 - \|\mathbf{S}_{fi}^{m,out} - \mathbf{S}_{fj}^{m,out}\|_2 \right| \quad (2)$$

where $\mathbf{S}^{m,out} = \mathbf{S}^{out} \circ \mathbf{M}$, denoting again that this loss is only computed over the visible part of the original sequence.

Bone Length Loss. We also enforce constant bone length of the whole generated sequence. Its main goal is to discourage the generator to explore solutions where the skeleton is not well formed. If we denote by $\bar{\mathbf{B}} = \{\bar{l}_1, \dots, \bar{l}_B\}$ the mean length of the B body bones computed over the visible part of the sequence, and by $\mathbf{B}_f = \{l_{f1}, \dots, l_{fB}\}$ the length of the bones at frame f , this loss is computed as

$$\mathcal{L}_{bone} = \sum_{f=1}^F \sum_{b=1}^B \|\bar{l}_b - l_{fb}\|_2 \quad (3)$$

Regularized Adversarial Loss. Our adversarial loss is based on the original GAN loss [14], with the R1 regularization described in [29]. Let G_θ be the generator network, parameterized by the variable θ , D_ψ be the discriminator network, parameterized by the variable ψ , and \mathbb{P}_o the distribution of input motion sequences. We can then write the Discriminator Loss as:

$$\begin{aligned} \mathcal{L}_D = & \mathbb{E}_{\mathbf{S}^{out} \sim \mathbb{P}_o} [\log(1 - D_\psi(G_\theta(\mathbf{S} \circ \mathbf{M})))] \\ & + \mathbb{E}_{\mathbf{S} \sim \mathbb{P}_o} [\log(D_\psi(x))] + \frac{\gamma}{2} \mathbb{E}_{\mathbf{S} \sim \mathbb{P}_o} [\|\nabla D_\psi(x)\|^2] \end{aligned} \quad (4)$$

The Generator Loss is as follows:

$$\mathcal{L}_G(\theta, \psi) = \mathbb{E}_{\mathbf{S}^{out} \sim \mathbb{P}_o} [\log(D_\psi(G_\theta(\mathbf{S} \circ \mathbf{M})))] \quad (5)$$

² $\mathbf{S}_{i::}$ denotes the i -th element of \mathbf{S} along the first axis.

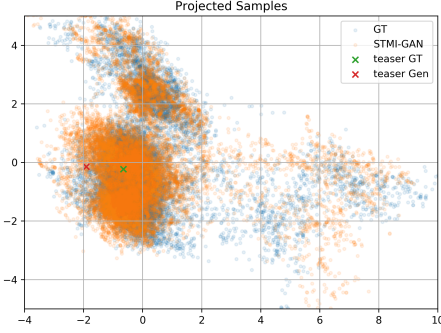


Figure 3. **LDA embedding.** Random samples (16K) from the Human3.6M Dataset, projected onto the LDA embedding. The figure shows the reprojected onto the first two dimensions, out of $D = 14$, that account for approximately 64% of the variability. Note that the sample distribution of our STMI-GAN network is very similar to the ground truth one. The crosses represent the generated and ground truth sequences depicted in Fig. 1.

Full Loss. The full loss \mathcal{L} consists of a linear combination of all previous partial losses:

$$\mathcal{L} = \lambda_r \mathcal{L}_{rec} + \lambda_l \mathcal{L}_{limb} + \lambda_b \mathcal{L}_{bone} + \lambda_D \mathcal{L}_D + \lambda_G \mathcal{L}_G \quad (6)$$

where λ_r , λ_l , λ_b , λ_D and λ_G are the hyper-parameters that control the relative importance of every loss term. Finally, we can define the following minimax problem:

$$G^* = \arg \min_G \max_{D \in \mathcal{D}} \mathcal{L}, \quad (7)$$

where G^* draws samples from the data distribution.

5. Metric for comparing motion sequences

As we have discussed above, standard metrics like L2 or the Dynamic Time Warping fail to capture the semantics across motion sequences. We therefore propose to evaluate the quality of the reconstructed results based on a metric that maps semantically similar motions to close locations in an embedded space. Furthermore, instead of performing a frame by frame comparison, we will assess the similarity of the original distribution in the training dataset, with that of the generated sequence. Concretely, our metric which we call LDA-SCC is computed as follows:

1. Train a Linear Discriminant Analysis (LDA) model for dimensionality reduction. The model is learned from random tensors $\text{vec}(\mathbf{S}) \in \mathbb{R}^{3FJ \times 1}$ of the training set, where $\text{vec}(\cdot)$ is the vectorization function. Let $\mathbf{D} \in \mathbb{R}^{3FJ \times D}$ be the LDA model. For our experiments we chose the LDA default of $D = \#classes - 1$, e.g. in the Human 3.6 dataset is $D = 14$.
2. Let \mathbf{S}^{out} and \mathbf{S}^{gt} be a generated motion sequence and its corresponding ground truth whose similarity is to be

compared. We first project them onto the LDA model, i.e. $\mathbf{s}_{lda}^{out} = \mathbf{D}^\top \text{vec}(\mathbf{S}^{out})$ and $\mathbf{s}_{lda}^{gt} = \mathbf{D}^\top \text{vec}(\mathbf{S}^{gt})$. Both \mathbf{s}_{lda}^{out} and \mathbf{s}_{lda}^{gt} are D -dimensional vectors.

3. Let ζ^{out} and ζ^{gt} be a set of samples of $\{\mathbf{s}_{lda}^{out}\}$ and $\{\mathbf{s}_{lda}^{gt}\}$, respectively. We calculate the Spearman correlation matrix between these projected distributions as:

$$SC = \frac{\text{ccov}(\text{rank}(\zeta^{gt}), \text{rank}(\zeta^{out}))}{\sigma_{\text{rank}(\zeta^{gt})} \sigma_{\text{rank}(\zeta^{out})}}, \quad (8)$$

where $\text{rank}(\cdot)$ is a ranking function, $\text{ccov}(\cdot, \cdot)$ the cross covariance and $\sigma_{\text{rank}(\cdot)}$ the standard deviations of the rank variables. $SC \in \mathbb{R}^{D \times D}$

4. Compute the average correlation between the relevant variables of the correlation matrix as $\text{scoeff} = \sum_{i=1}^D SC_{ii} / D$,

The resulting metric is a coefficient in $[-1, 1]$. A correlation of -1 means that the variables are inversely correlated, 0 that they are uncorrelated and 1 perfectly correlated. This metric is independent of the dimension of the embedding space and it only considers if the samples preserve their relative position. This measures how mixed are the samples after passing through the network, 1 meaning the two variables being compared are monotonically related.

6. Implementation Details

We next describe the blocks of our architecture. *We plan to make our code publicly available.*

6.1. GAN Implementation

Frame Autoencoder.

The Frame Encoder (Fig. 4-left) is a fully connected network with several identical sequential blocks. Each block contains two consecutive fully connected layers, and an attention mechanism at the end. The fully connected layers can also be seen as 1D convolutions with kernel size 1 along the time dimension. The attention is performed by applying a mask over the output of the block. The mask is a linear transformation of the input to the block, followed by a sigmoid activation. This attention mechanism is similar to the gates described in [3]. After the blocks, a final linear transformation and an attention are applied. The architecture is similar to a VAE[23], but without the Gaussian constraints over the output of the encoder. The decoder network is simply a symmetrical network to the encoder, with the same number of blocks and layers, but independent parameters.

Generator U-Blocks.

The goal of the generator is to preserve the shape of the sequence through the network and produce an output that should be indistinguishable from an input. To accomplish this, we use U shaped blocks inspired in [32]. These blocks

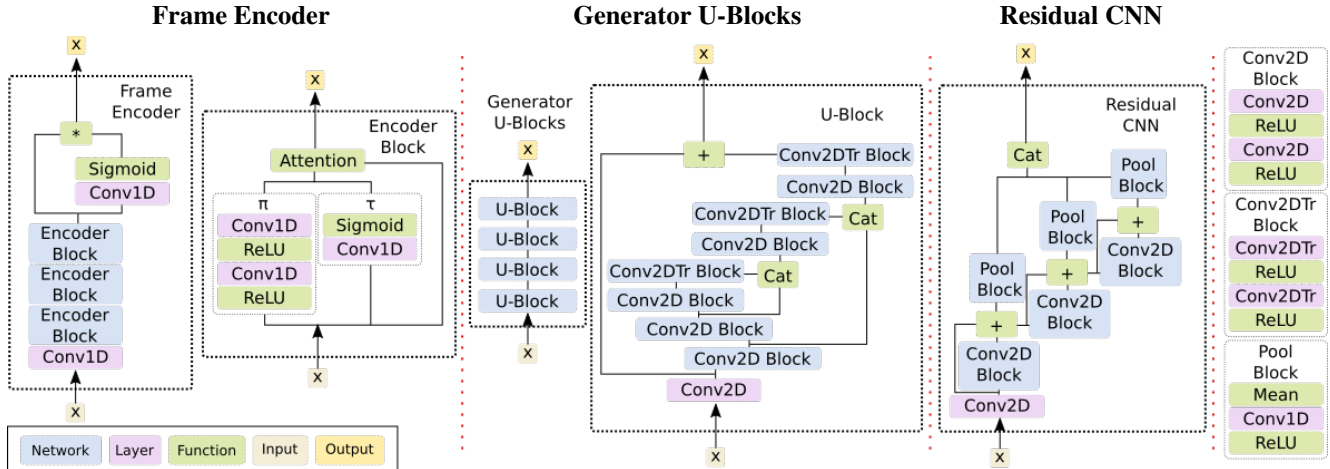


Figure 4. **Details of the architecture.** From left to right: Frame Encoder; Generator U-Blocks; Residual CNN. In each case we plot the general view of the block (left) and the fine detail of the structural elements (right). The Attention function is defined as: $att(x, \pi, \tau) = (\pi * \tau) + (x * 1 - \tau)$. The Conv2DTr denotes Convolution 2D Transpose, also called deconvolution.

(see Fig. 4-center) use convolutions to halve the spatial resolution of the input in each layer, until it reaches a small representation. Then a transposed convolution is used to double the resolution until it reaches again the same dimensions as the input. A key component in this architecture, are the skip connections that connect from the output of the convolutional layers to the input of the deconvolutional layers. We can think of this architecture as an iterative refinement, in which the output of a block is refined by the next block to produce a better final output.

Residual CNN. A discriminator is essentially a classifier network that attempts to distinguish real samples from "fake" generated samples. For that reason we designed the architecture of our discriminator inspired on ResNet[17] and DenseNet[19]. Our network (Fig. 4-right) branches in three discriminators, and each discriminator has a classifier. The classifiers share the same architecture but have separate parameters. Each classifier has several consecutive blocks with two convolutional layers and additive residual connections, similar to ResNet. The outputs of each block are also transformed and then concatenated into a tensor. The final output is the concatenation of the outputs of all blocks. This output is finally passed onto a fully connected network that assigns a score.

Sequence Alignment. Since we are working over an absolute coordinate system, the sequences can happen in a wide range of numbers depending on the dataset. To improve the robustness of the generator we align the sequences by subtracting the position of the hip joint in the first frame to all the joints in the sequence. Then the skeleton is rotated to always face the in the same direction. This alignment is performed just before entering the frame encoder, and is reversed just after exiting the frame decoder. Note that this

Model	\mathbb{E}_{dist}	min_{dist}	LDA-SCC
NoGAN	4.1489	2.6036	0.5104
Enc disc	3.6837	2.3768	0.5747
+EDM disc	4.0130	2.4921	0.5521
+Motion disc	3.5438	2.2734	0.6003
STMI-GAN	3.5355	2.2780	0.6051

Table 1. **Ablation Study.** LDA based metrics for different configurations of our model.

does not affect the capacity of our network to forecast sequences in global coordinates, and it does not require any preprocessing of the data.

7. Experiments

Datasets. In the experimental section we mainly use the Human3.6M [20] dataset. We will use this dataset to test our approach and to compare it to other methods and baselines. We will also provide qualitative results on the Microsoft Research 12 [12] to show the capabilities of our model to work on different data.

7.1. Ablation Study

We next run an ablation study, using always the same generator network, but training it with different losses. As we argued in previous sections, we aim to capture the distribution of the Ground Truth (GT) data, and each component in the architecture was designed with this purpose. Our hypothesis is that an adversarial loss is better than L2 and geometric losses to train a generative network. Even more, we argue that the complexity of the discriminator network should be correlated with a better result in the generated sequences.

We use three different measurements in the LDA em-

Model	Milliseconds									
	200	400	600	800	1000	1200	1400	1600	1800	2000
Res.Sup[28]	359.23	619.96	803.74	915.79	1011.26	1061.15	1111.69	1139.47	1224.40	1304.37
NoGAN	439.91	668.76	826.08	923.73	980.57	1005.31	1055.06	1104.52	1140.25	1180.90
STMI-GAN	460.35	760.87	944.68	992.54	1041.13	1098.20	1216.18	1303.32	1344.78	1417.00

Table 2. **L2 distance between EDM matrices.** Comparison of [28] with our baselines using the L2 metric. The NoGAN approach, which was specifically trained to minimize an L2 loss is the most accurate in the long-term. Note that STMI-GAN also estimates the full position, but this is not considered in this experiment.

bedded space to test our hypothesis: 1) \mathbb{E}_{dist} : Average L2 distance between GT and generated sequences in the embedded LDA space. It tells in average how different are the generated sequences from the ground truth. 2) min_{dist} : The minimal distance. Given the stochastic nature of future prediction, the estimated sequence might not be totally correct, but the generator might still be able to generate a realistic sequence. To measure this intrinsic capacity, we consider min_{dist} as the average minimal distance from every GT sequence to all generated sequences. This distance is similar to the Chamfer distance used to measure the similarity of point clouds. 3) LDA-SCC: with the Spearman coefficient on the projected LDA space, we can capture a general notion on how similar the two distributions are. This metric was thoroughly explained in Sec.5.

Our tested models are: NoGAN: generator network trained with the reconstruction loss over the whole sequence, and no adversarial loss. Enc disc: is the same network, but using the encoder discriminator as loss for the generated part. +EDM disc: the network is trained using both the encoder and the EDM discriminators. +Motion disc: the network is trained using the encoder and motion discriminator. STMI-GAN: is the full network, trained with all joint discriminators. As summarized in Table 1, the model trained without an adversarial loss performs the worst, with the higher distances, and the lowest correlation value. On the other end of the spectrum, our model with the three proposed discriminators performs the best. We should note that the scores of the networks can be ordered by its increasing complexity. Every component seems to be adding information to the generator, as the LDA-SCC increases with each addition. We then discard the hypothesis that some of the adversarial losses are not contributing. Thanks to these measurements, and our qualitative assessment we can conclude that our approach is indeed correct.

7.2. Motion Prediction

In this section we compare our approach to [28], which one of the baseline works in the state of the art. From this work, we are using the residual supervised model, which is a sequence-to-sequence model with residual connections and uses the labels as part of the inputs. Since the Res.Sup. model is based on angles, we perform forward kinematics to recover the actual pose in the Cartesian space, to be able

to compare it to our approach.

Quantitative Evaluation. We have previously argued that L2 metric over the Cartesian space, or over angles is a poor metric, and because of that we introduced the LDA-SCC metric in the previous section. Unfortunately, we could not apply the metric to the baseline model. The deterministic design of the Res.Sup. approach makes it impossible to perform the extensive sampling required to perform a numerically stable correlation analysis. For that reason, we introduce a metric that is more similar to theirs. The EDM distance metric, is the L2 distance between the EDM projected sequences. The EDM is a rotation and translation invariant representation, and in this regard it is very similar to the angles representation used in their approach.

The residual model essentially copies the pose from the last frame, and only predicts the update in motion. If we are measuring in L2 this should give an advantage in the short term, because the human motion is relatively slow and simply copying the pose is often a good guess. In fact in Tab. 2 we can see that the Res.Sup. model has the lowest error below the 800ms. However, in the long run we should be better off with a model that is capable of learning to reproduce whole sequences instead of predicting updates frame by frame. As we can observe, our NoGAN model performs better than the baseline from 1000ms onward. Since this model was trained to minimize L2 over the generated sequence, these results are to be expected. Nonetheless, we know from the ablation study that our STMI-GAN model can capture better the complexity of the human motion. We argue that it shows worse results in this metric only because of the inherent stochasticity of the prediction problem and the L2 metric on angles, Cartesian space and even over EDMs is unable to grasp the semantics of the sequences. Also, recall that STMI-GAN solves an additional complexity as it also estimates absolute body position, which was eliminated in this analysis. To further demonstrate this point, we propose a qualitative evaluation of the models.

Qualitative Evaluation. We conducted evaluation with 15 person and four distinct surveys, all of them following the same scheme: a prediction model vs the ground truth. In the first two surveys we tested the baseline Res.Sup and STMI-GAN, to perform relative motion prediction. In the case of our model we removed the translation from the prediction to

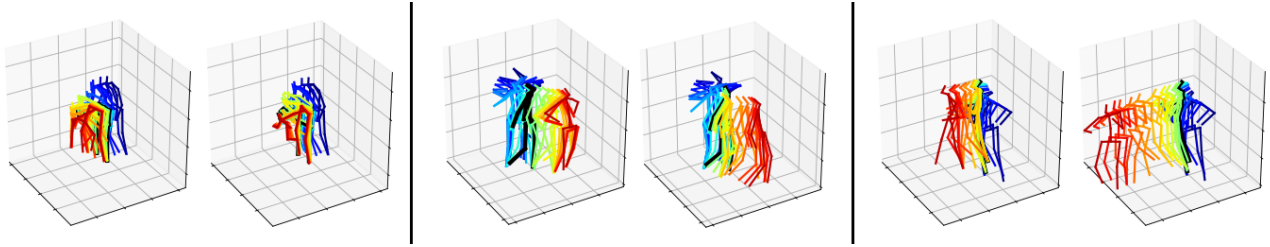


Figure 5. **Example result.** Three examples of the predicted motions (left: ground truth, right: predicted). The bluish colors are the part of the sequence that is observed. The prediction starts after the black skeleton and corresponds to the yellow-reddish colors.

Model	Motion	Min	Avg	Max
Res.Sup.[28]	Rel.	6.25%	31.88%	40.63%
STMI-GAN	Rel.	25.00%	33.54%	40.63%
NoGAN	Abs.	9.38%	31.46%	62.50%
STMI-GAN	Abs.	15.63%	38.39%	62.50%

Table 3. **Human Evaluation.** Percentage of times that a human evaluator thought a generated sequence was real.

make it comparable. The last two surveys assess the absolute motion prediction. We use our NoGAN model as baseline vs our STMI-GAN model. In these surveys our goal is to obtain a 50% chance of being classified as real. More than 50% would mean that the model is "more realistic" than the ground truth. As we can observe in Tab. 3 the results have a wide range of values. This is due to the fact that the survey was sent to a diverse audience. The max score tells us what a naive guess would be. On the other hand, the min score would tell us what a highly trained guess would be. We can see that the baselines perform in a similar range of average values as our model, our model being bit better. However, the baselines perform very poor to the trained eye, as the min score tells us. It is worth to note that while the relative motion prediction is an easier problem compared to the absolute motion prediction, the average score of our STMI-GAN is lower in the relative setting. This suggests that the relative motion problem is both harder for machine learning models and for humans. Also, the highest score on the surveys is in the max of the STMI-GAN in absolute prediction. This implies that some individuals were very convinced by the results of our model.

Fig.5 shows three examples. The sequence on the left is easy to predict, just continuing the motion of picking up things off the floor. The sequence on the center is a bit harder, as it is easy to guess that the person will continue walking, but the person halts after a couple of steps, and this is unexpected. The sequence on the right is challenging, because just before the generator begins its forecast, the person stops. This makes it hard to predict as the uncertainty rises and many options are plausible. We can see that the generator in fact guessed the action (walking) and the correct direction, but the speed of the motion is not accurate. We consider it however a good guess given the input.

Problem	Linear Int	LR-Kalman[7]	NoGAN	STMI-GAN
Random Occl.	18.74	24.26	91.63	29.41
Structured Occl.	71.03	108.20	251.80	49.95
Missing Frames	60.73	82.28	176.31	60.28
Noisy Transm.	40.46	90.31	170.94	42.22

Table 4. **Occlusion Completion.** We test different types of occlusion, concretely: **Random Occlusions:** joints occluded at random in each frame. **Structured Occlusions:** body parts, consisting on contiguous joints, are occluded at random in each frame. **Missing Frames:** entire frames are occluded at random. **Missing transmission:** data points in any dimension are occluded at random. The table reports the L2 distance over EDMs.

7.3. Occlusion Completion

Finally, in Table 4 we report the robustness to different types of occlusion. In every test we used 80% of occlusion, *i.e.* we are trying to recover a sequence conditioning only on 20% of the data. We compute the L2 distance over the EDMs similar to the previous section. The STMI-GAN model is particularly robust to structured occlusions, we hypothesize that this is because it was trained to produce anthropomorphic guesses. When the occlusions happen at random, linear interpolation and filtering strategies are also good approaches, but depending on the nature of the occlusion we may need a more robust model.

8. Conclusions

We have presented a novel GAN architecture to predict 3D human motion from historical 3D skeleton poses. We have extended existing works, by also forecasting (beyond 2 seconds) the absolute position of the body. We have formulated our problem as an inpainting task in spatio-temporal volumes. In order to capture the essence and semantics of the human motion, the training of our network has been mostly ruled by three independent critics, that encourage the generation of motion sequences with similar geometric distributions than ground true ones. Since L2 is known not to be adequate to compare motion sequences, we have also proposed a new metric which aims to maximize the distributions over an embedded space. Experimental results on Human3.6M show the effectiveness of our model to generate highly realistic human motion predictions.

References

- [1] A. Agudo and F. Moreno-Noguer. Dust: Dual union of spatio-temporal subspaces for monocular multiple object 3d reconstruction. **2**
- [2] I. Akhter, T. Simon, S. Khan, I. Matthews, and Y. Sheikh. Bilinear spatiotemporal basis models. *ACM Transactions on Graphics (TOG)*, 31(2):17, 2012. **2**
- [3] A. V. M. Barone. Low-rank passthrough neural networks. *arXiv preprint arXiv:1603.03116*, 2016. **5**
- [4] E. Barsoum, J. Kender, and Z. Liu. Hp-gan: Probabilistic 3d human motion prediction via gan. *arXiv preprint arXiv:1711.09561*, 2017. **2**
- [5] Y. Bengio, L. Yao, G. Alain, and P. Vincent. Generalized denoising auto-encoders as generative models. In *Advances in Neural Information Processing Systems*, pages 899–907, 2013. **3**
- [6] M. Brand and A. Hertzmann. Style machines. In *Proceedings of the 27th annual conference on Computer graphics and interactive techniques*, pages 183–192. ACM Press/Addison-Wesley Publishing Co., 2000. **2**
- [7] M. Burke and J. Lasenby. Estimating missing marker positions using low dimensional kalman smoothing. *Journal of biomechanics*, 49(9):1854–1858, 2016. **8**
- [8] J. Bütepage, M. J. Black, D. Kragic, and H. Kjellström. Deep representation learning for human motion prediction and classification. In *IEEE Conference on Computer Vision and Pattern Recognition (CVPR)*, page 2017. IEEE, 2017. **2**
- [9] J. Bütepage, H. Kjellström, and D. Kragic. Anticipating many futures: Online human motion prediction and generation for human-robot interaction. In *2018 IEEE International Conference on Robotics and Automation (ICRA)*, pages 1–9. IEEE, 2018. **1, 2**
- [10] K. Cho, B. Van Merriënboer, C. Gulcehre, D. Bahdanau, F. Bougares, H. Schwenk, and Y. Bengio. Learning phrase representations using rnn encoder-decoder for statistical machine translation. *arXiv preprint arXiv:1406.1078*, 2014. **2**
- [11] H. Coskun, D. J. Tan, S. Conjeti, N. Navab, and F. Tombari. Human motion analysis with deep metric learning. *arXiv preprint arXiv:1807.11176*, 2018. **3**
- [12] S. Fothergill, H. Mentis, P. Kohli, and S. Nowozin. Instructing people for training gestural interactive systems. In *Proceedings of the SIGCHI Conference on Human Factors in Computing Systems*, pages 1737–1746. ACM, 2012. **6**
- [13] K. Fragkiadaki, S. Levine, P. Felsen, and J. Malik. Recurrent network models for human dynamics. In *Proceedings of the IEEE International Conference on Computer Vision*, pages 4346–4354, 2015. **1, 2**
- [14] I. Goodfellow, J. Pouget-Abadie, M. Mirza, B. Xu, D. Warde-Farley, S. Ozair, A. Courville, and Y. Bengio. Generative adversarial nets. In *Advances in neural information processing systems*, pages 2672–2680, 2014. **4**
- [15] L.-Y. Gui, Y.-X. Wang, X. Liang, and J. M. Moura. Adversarial geometry-aware human motion prediction. In *ECCV*, pages 823–842, 2018. **1, 2, 3**
- [16] I. Gulrajani, F. Ahmed, M. Arjovsky, V. Dumoulin, and A. C. Courville. Improved training of wasserstein gans. In *Advances in Neural Information Processing Systems*, pages 5767–5777, 2017. **2**
- [17] K. He, X. Zhang, S. Ren, and J. Sun. Deep residual learning for image recognition. In *Proceedings of the IEEE conference on computer vision and pattern recognition*, pages 770–778, 2016. **6**
- [18] A. Hernandez Ruiz, L. Porzi, S. Rota Bulò, and F. Moreno-Noguer. 3d cnns on distance matrices for human action recognition. In *Proceedings of the 2017 ACM on Multimedia Conference*, pages 1087–1095. ACM, 2017. **4**
- [19] G. Huang, Z. Liu, L. Van Der Maaten, and K. Q. Weinberger. Densely connected convolutional networks. In *CVPR*, volume 1, page 3, 2017. **6**
- [20] C. Ionescu, D. Papava, V. Olaru, and C. Sminchisescu. Human3.6m: Large scale datasets and predictive methods for 3d human sensing in natural environments. *IEEE Transactions on Pattern Analysis and Machine Intelligence*, 36(7):1325–1339, jul 2014. **1, 6**
- [21] A. Jain, A. R. Zamir, S. Savarese, and A. Saxena. Structural-rnn: Deep learning on spatio-temporal graphs. In *Proceedings of the IEEE Conference on Computer Vision and Pattern Recognition*, pages 5308–5317, 2016. **1, 2**
- [22] A. Karpathy, J. Johnson, and L. Fei-Fei. Visualizing and understanding recurrent networks. *arXiv preprint arXiv:1506.02078*, 2015. **2**
- [23] D. P. Kingma and M. Welling. Auto-encoding variational bayes. *arXiv preprint arXiv:1312.6114*, 2013. **3, 5**
- [24] T. Kucherenko, J. Beskow, and H. Kjellström. A neural network approach to missing marker reconstruction in human motion capture. *arXiv preprint arXiv:1803.02665*, 2018. **2**
- [25] A. M. Lehrmann, P. V. Gehler, and S. Nowozin. Efficient nonlinear markov models for human motion. In *Proceedings of the IEEE Conference on Computer Vision and Pattern Recognition*, pages 1314–1321, 2014. **2**
- [26] C. Li, Z. Zhang, W. S. Lee, and G. H. Lee. Convolutional sequence to sequence model for human dynamics. In *Proceedings of the IEEE Conference on Computer Vision and Pattern Recognition*, pages 5226–5234, 2018. **2**
- [27] U. Mall, G. R. Lal, S. Chaudhuri, and P. Chaudhuri. A deep recurrent framework for cleaning motion capture data. *arXiv preprint arXiv:1712.03380*, 2017. **2**
- [28] J. Martinez, M. J. Black, and J. Romero. On human motion prediction using recurrent neural networks. In *2017 IEEE Conference on Computer Vision and Pattern Recognition (CVPR)*, pages 4674–4683. IEEE, 2017. **1, 2, 7, 8**
- [29] L. Mescheder, A. Geiger, and S. Nowozin. Which training methods for gans do actually converge? In *International Conference on Machine Learning*, pages 3478–3487, 2018. **4**
- [30] V. Pavlovic, J. M. Rehg, and J. MacCormick. Learning switching linear models of human motion. In *Advances in neural information processing systems*, pages 981–987, 2001. **2**
- [31] A. Radford, L. Metz, and S. Chintala. Unsupervised representation learning with deep convolutional generative adversarial networks. *arXiv preprint arXiv:1511.06434*, 2015. **3**

- [32] O. Ronneberger, P. Fischer, and T. Brox. U-net: Convolutional networks for biomedical image segmentation. In *International Conference on Medical image computing and computer-assisted intervention*, pages 234–241. Springer, 2015. 5
- [33] I. Sutskever, G. E. Hinton, and G. W. Taylor. The recurrent temporal restricted boltzmann machine. In *Advances in neural information processing systems*, pages 1601–1608, 2009. 2
- [34] I. Sutskever, O. Vinyals, and Q. V. Le. Sequence to sequence learning with neural networks. In *Advances in neural information processing systems*, pages 3104–3112, 2014. 2
- [35] G. W. Taylor and G. E. Hinton. Factored conditional restricted boltzmann machines for modeling motion style. In *Proceedings of the 26th annual international conference on machine learning*, pages 1025–1032. ACM, 2009. 2
- [36] G. W. Taylor, G. E. Hinton, and S. T. Roweis. Modeling human motion using binary latent variables. In *Advances in neural information processing systems*, pages 1345–1352, 2007. 2
- [37] R. Urtasun, D. J. Fleet, and P. Fua. 3d people tracking with gaussian process dynamical models. In *Computer Vision and Pattern Recognition, 2006 IEEE Computer Society Conference on*, volume 1, pages 238–245. IEEE, 2006. 2
- [38] R. Urtasun, D. J. Fleet, A. Geiger, J. Popović, T. J. Darrell, and N. D. Lawrence. Topologically-constrained latent variable models. In *Proceedings of the 25th international conference on Machine learning*, pages 1080–1087. ACM, 2008. 2
- [39] J. M. Wang, D. J. Fleet, and A. Hertzmann. Gaussian process dynamical models for human motion. *IEEE transactions on pattern analysis and machine intelligence*, 30(2):283–298, 2008. 2
- [40] G. Xia, H. Sun, B. Chen, Q. Liu, L. Feng, G. Zhang, and R. Hang. Nonlinear low-rank matrix completion for human motion recovery. *IEEE Transactions on Image Processing*, 27(6):3011–3024, 2018. 2
- [41] R. A. Yeh, C. Chen, T.-Y. Lim, A. G. Schwing, M. Hasegawa-Johnson, and M. N. Do. Semantic image inpainting with deep generative models. In *CVPR*, volume 2, page 4, 2017. 3
- [42] J. Yu, Z. Lin, J. Yang, X. Shen, X. Lu, and T. S. Huang. Generative image inpainting with contextual attention. *arXiv preprint*, 2018. 3